Chemical Engineering Journal 514 (2025) 163003

Contents lists available at ScienceDirect

Chemical Engineering Journal

journal homepage: www.elsevier.com/locate/cej

Gangue-based Cu/SSZ-13 zeolites with controllable Al distribution as robust selective catalytic reduction (SCR) catalysts

Tongrui Liu [a,b], Linying Wang [a], Linhai He [a,b], Huihui Chen [a,b], Dong Fan [a], Dali Zhu [a], Miao Yang [a], Peng Tian [a,*], Zhongmin Liu [a,b,**]

[a] National Engineering Research Center of Lower-Carbon Catalysis Technology, Dalian National Laboratory for Clean Energy, Dalian Institute of Chemical Physics, Chinese Academy of Sciences, Dalian 116023 Liaoning, China
[b] University of Chinese Academy of Sciences, Beijing 100049 Beijing, China

ARTICLE INFO

Keywords:
Cu/SSZ-13
NH_3-SCR
Zeolite synthesis
Coal gangue
Solid waste

ABSTRACT

An eco-friendly and cost-effective approach for the fast synthesis of SSZ-13 with tunable Al distribution has been developed by utilizing coal gangue as an inorganic source under the assistance of embryonic CHA zeolite. The proportion of Al species with close spatial proximity (Al_{pairs} and Al_{close}) in SSZ-13 can reach as high as 73 %. The Al pairs-enriched Cu/SSZ-13 (named Cu/GS6) facilitates the formation of hydrothermally stable Cu^{2+}-2Z species and shows a broad NH_3-SCR working temperature window (T_{90}: 175–600 °C, GHSV = 300,000 h^{-1}) and robust resistance to hydrothermal aging at 800 °C. Both framework Al distribution and structural integrity are demonstrated to be key factors determining the catalytic activity and hydrothermal stability of Cu/SSZ-13. The (Al_{pairs} and Al_{close}) species are more efficient than isolated Al species for the migration of active Cu species, contributing to the superior low-temperature activity of Cu/GS6. Moreover, it is revealed that structural defects in zeolites lead to aggravated framework dealumination during Cu-based catalyst preparation and hydrothermal aging, which should be minimized to enhance the catalyst stability. The efficient utilization of industrial solid waste for controllable synthesis of SSZ-13 and the insights into the synthesis-property-performance relationships are expected to prompt the development of high-performance NH_3-SCR catalysts and their application.

1. Introduction

Coal gangue, an industrial solid waste produced during coal mining and washing, accounts for approximately 10–15 % of the total output of raw coal [1]. The massive accumulation of coal gangue leads to environmental problems and geological hazards. As the main components of coal gangue are SiO_2 and Al_2O_3, the conversion of coal gangue into functional materials, such as zeolites, adsorbents and ceramics, has been attracting considerable interest. This provides a cost-effective and eco-friendly approach to the manufacturing of materials with high value and would promote their practical applications.

Zeolite materials are important solid catalysts owing to their unique shape-selectivity and adjustable acidity [2]. Among zeolites, small pore zeolite SSZ-13 (CHA type) has received great attention in recent years, as Cu-based SSZ-13 (Cu/SSZ-13) exhibits promising catalytic performance for methane to methanol [3] and NH_3-selective catalytic reduction of NO*x* (NH_3-SCR). Although Cu/SSZ-13 has been commercialized as NH_3-SCR catalyst for diesel engine exhaust treatment [2,4], it is still highly desirable to develop eco-friendly strategy to high-performance Cu/SSZ-13 catalyst with improved SCR catalytic activity, hydrothermal durability and widened operation window, in order to meet the increasingly stringent emission standards.

The atomic-level understanding of the function of Cu active sites in Cu/SSZ-13 provides guidance for NH_3-SCR mechanism elucidation and catalyst optimization. It has been demonstrated that the NH_3-SCR reaction at low temperature (~150–250 °C) occurs on the NH_3-solvated Cu cations in zeolite nanocages via the Cu(I)/Cu(II) catalytic cycle. The transfer of active Cu species is crucial for the reaction efficiency, as the key intermediates involve the pairing of Cu species within the cages [5,6]. When the temperature was higher than 250 °C, Cu-NH_3 complexes (only stable at low temperature) will dissociate, the transfer of Cu species becomes difficult, and the NH_3-SCR reaction occurs on the single

* Corresponding author.
** Corresponding author at: National Engineering Research Center of Lower-Carbon Catalysis Technology, Dalian National Laboratory for Clean Energy, Dalian Institute of Chemical Physics, Chinese Academy of Sciences, Dalian 116023, Liaoning, China.
E-mail addresses: tianpeng@dicp.ac.cn (P. Tian), liuzm@dicp.ac.cn (Z. Liu).

https://doi.org/10.1016/j.cej.2025.163003
Received 4 December 2024; Received in revised form 18 April 2025; Accepted 22 April 2025
Available online 23 April 2025

isolated Cu species. There are two active centers in Cu/SSZ-13: isolated Cu^{2+}-2Z and $[Cu(OH)]^{+}$-Z [5]. The Cu^{2+}-2Z species are anchored to Al pairs in the framework and hence possess better high-temperature stability owing to its interaction with Al pairs in the framework. Whereas for $[Cu(OH)]^{+}$-Z, the relatively weak interaction with the framework endows their higher mobility, and thus enhanced low-temperature activity. The high mobility of $[Cu(OH)]^{+}$-Z, however, would induce its conversion to CuO_x clusters when exposed to steam at high temperature, causing loss of active sites and dealumination/degradation of the framework. There is thus a trade-off between the hydrothermal stability and low-temperature activity of Cu/SSZ-13 catalyst.

Recently, the importance of Al (acid) density of Cu/SSZ-13 support has also been revealed, which affects the dynamic migration of Cu species at low temperature and their reactivity [5,7–9]. Based on Cu/SSZ-13 catalysts of varying framework Al density, Gounder et al. demonstrated that increasing the Al density can lead to the increase of Cu(I) species proportion and Cu(I) oxidation rate constants [8]. Fu et al. reported that the spatial distribution of framework Al sites affects the inter-cage diffusion and reactivity of $Cu(I)(NH_3)_2$ [9]. Wu et al. found that the Brönsted acid sites (BASs) have a strong kinetic correlation with the oxidation half-cycle of Cu species at low temperatures. The loss of BASs will hinder the hydrolysis of $Cu(II)(NH_3)_4$ and the migration of $Cu(II)(OH)(NH_3)_3$ [7]. Chen et al. reported that the increase of paired Al in SSZ-13 can promote the formation of Cu^{2+}-2Z, and suppress the loss of active Cu species and framework dealumination. Our works based on Cu/SAPO-34 also revealed the significant impact of acidity on low-temperature activity [10]. Moreover, the BASs were proposed to contribute to NH_3-SCR reaction by decomposing $HONO/H_2NNO$ intermediates into N_2 and H_2O [11].

The above works imply that the Al distribution in parent SSZ-13 affects the Cu distribution, mobility and reactivity of Cu species. The synthesis of SSZ-13 with controllable Al distribution can adjust the Cu distribution and thus regulate the catalytic activity and hydrothermal stability. Hitherto, the strategies developed for adjusting the Al distribution in SSZ-13 include modulating alkali metal ions [12,13], the choice of organic structure-directing agents (OSDAs) [14] and employing nucleation seeds [15]. Gounder et al. explored the cooperation/competition between Na^{+}/K^{+} and N,N,N-trimethyl-1-adamantammonium hydroxide (TMAdaOH) for the occupation in microporous voids of SSZ-13, and rationalized the differences of Na^{+} and K^{+} in stabilizing different Al configurations. However, the synthesis of SSZ-13 generally suffers the excessive usage of expensive TMAdaOH or long crystallization period, especially when attempting to enhance the proportion of framework Al pairs. It would be valuable to develop a highly efficient and cost-effective synthetic strategy for SSZ-13 with controllable Al distribution.

In this work, we report the eco-friendly and fast synthesis of SSZ-13 for NH_3-SCR by utilizing dealuminated coal gangue as an inorganic source under an ultra-low TMAdaOH usage (OSDA/Si = 0.045–0.072). Coal gangue was previously used for the synthesis of zeolites A and X (Si/Al = 1 ~ 3) owing to its low-silica composition [16,17]. A treatment method was developed herein to prepare dealuminated coal gangue with high reactivity and appropriate composition for SSZ-13 synthesis. The Al distribution of SSZ-13 can be facilely modulated by varying the NaOH dosage in the initial gel. The relations between the Al distribution and Cu species as well as the acidity, defects and catalytic performance were investigated to rationalize the superior catalytic activity and hydrothermal durability of Cu/SSZ-13 for NH_3-SCR reaction. Based on the established correlation of synthesis-property-performance, synthesis regulation is proposed for the preparation of high-performance Cu/SSZ-13 catalyst with enhanced hydrothermal stability.

2. Experimental

2.1. Chemical reagents

The chemical regents used include sodium aluminate (48 wt% Al_2O_3, 36 wt% Na_2O, Aladdin), silica gel (99 wt%, Qingdao Meigao Reagent Co.), sodium hydroxide (NaOH, 99.9 wt%, Aladdin), tetraethylorthosilicate (TEOS, 99 wt%, Kermel), aluminum isopropoxide (AIP, ≥98 wt%, Aladdin), hydrochloric acid (HCl, 36 wt%, Tianjin Damao Chemical Reagent Co.), TMAdaOH (25 wt% in H_2O, Annaiji), ammonium chloride (NH_4Cl, 99 wt%, Tianjin Damao Chemical Reagent Co.), cobaltous nitrate ($Co(NO_3)_2{\cdot}6H_2O$, 99 wt%, Xilong Chemical Reagent Co.), copper acetate monohydrate (Cu(CH3COO)2·H2O, 99 wt%, Tianjin Damao Chemical Reagent Co.). Coal gangue was obtained from Shanxi Yangmei Group Chemical Energy Co., Ltd.

2.2. Pretreatment of coal gangue

The bulk coal gangue was first grinded mechanically to reduce particle sizes (less than 40 mesh) and calcined in air at 750 ℃ for 6 h. Then it was dispersed into water and milled at 550 rpm/min for 360 min using a planetary ball mill with agate beads mixture in diameter of 3, 6 and 10 mm. After milling, hydrochloric acid solution (20 wt% HCl) was added into the mud to obtain a mixture (solid/liquid ratio of 1 g/10 mL). The acid treatment was carried out under stirring at 95 ℃ for 6 h. Finally, the solid was separated by centrifugation, washed and dried at 100 ℃. The material after pretreatment was named deAl-G.

2.3. Synthesis of SSZ-13

An embryonic-CHA-zeolite solution was first prepared with a gel molar composition of 100TEOS: 6.4AIP: 7.2TMAdaOH: 2064H_2O according to our previous work [18]. The typical gangue-based SSZ-13 synthesis was carried out as follows. NaOH, deionized water, sodium aluminate (if needed) and TMAdaOH were mixed to obtain a clear solution. After the addition of deAl-G and stirring for 30 min, embryonic zeolite solution (10 wt% addition based on the silica mass of deAl-G) was added, and the resulting mixture was stirred for another 2 h and then transferred into an autoclave. The final gel molar composition for each sample was listed in Table 1. The crystallization was performed under rotation at 175 °C for 12 h. Then the product was separated by centrifugation, washing, drying and calcination in air at 550 °C for 5 h. The sample was named GS*x* (*x* refers to synthesis entry in Table 1). Solid yield was calculated based on the mass of silica and alumina.

2.4. Catalyst preparation

NH_4-type samples were prepared by ion exchange of the calcined sample with NH_4Cl solution (1.0 M, solid/liquid = 1 g/20 mL) at 80 ℃ for 2 h and the procedure was repeated three times. Cu/SSZ-13 catalysts were obtained by ion exchange of NH_4-type samples with $Cu(CH_3COO)_2$ solution (0.01 mol/L and solid/liquid = 1 g/50 mL) at 80 ℃ for 3 h, followed by centrifugation, washing, drying, and calcination in air at 550 ℃ for 5 h. The fresh catalyst was named Cu/GS*x*.

For hydrothermal aging, the catalyst was treated at 750 °C (or 800 °C) for 16 h under 12.5 % H_2O/ air with a GHSV of 100,000 h^{-1}. The aged catalysts were named HTA-Cu/GS*x*.

Co ion exchange was carried out at 80 °C for 12 h using NH_4-type sample and $Co(NO_3)_2$ solution (0.05 mol/L). The procedure was repeated three times to ensure complete exchange.

2.5. Characterization and catalyst activity test

The detailed characterization, catalyst activity test and kinetic test are given in the Supplementary Information.

Table 1
Synthesis conditions, product compositions and solid yields (175 °C, 12 h).

Sample	Gel molar composition[a]			Product				Co/Al[d]	Al_{iso}[d]
	x Al_2O_3	*y* NaOH	*z* OSDA	Phase[b]	Si/Al	Na/Al	Yield		
GS1	2.2	18.2	7.2	CHA	18.5	0.324	78.9 %	–	–
GS2	5.1	9.6	7.2	CHA	10.2	0.378	93.4 %	–	–
GS3	6.4	3.6	7.2	CHA	9.1	0.194	86.4 %	0.21	57.2 %
GS4	6.4	5.4	7.2	CHA	8.3	0.318	91.4 %	0.24	51.6 %
GS5	6.4	9.6	7.2	CHA	8.0	0.328	93.0 %	0.30	39.8 %
GS6	6.4	13.0	7.2	CHA	8.2	0.329	91.2 %	0.36	27.2 %
GS7	6.4	18.2	7.2	CHA	8.2	0.262	81.1 %	–	–
GS8	6.4	9.6	4.5	CHA	8.0	0.335	91.2 %	–	–
GS9	6.4	13.0	4.5	No[c]	–	–	–	–	–
GS10[c]	6.4	13.0	7.2	No[c]	–	–	–	–	–

[a] The molar composition of final gel (containing embryonic-zeolite solution) was $100SiO_2$:*x*Al_2O_3:*y*NaOH:*z*TMAdaOH:$2063H_2O$ (exception for GS1, H_2O/SiO_2 = 42.5). Note that deAl-G-1, deAl-G-2 and deAl-G-3 with different SARs (Table S1) were used as sources for the synthesis of GS1, GS2 and GS3-GS10, respectively.
[b] Samples GS1-GS8 contain small amount of quartz residue from coal gangue.
[c] No crystallization occurred. No addition of embryonic-zeolite solution for GS10.
[d] Co/Al atomic ratio: calculated based on Co^{2+} exchange results. $Al_{isolated}$=($Al_{framework}$ –2Co)*100 %/$Al_{framework}$.

3. Results and discussion

3.1. Controllable dealumination and activation of coal gangue

The coal gangue used in this work is raw ore, which mainly contains lamellar kaolin and quartz phases (Fig. S1). Composition analysis (Table S1) shows that coal gangue consists of SiO_2, Al_2O_3, Fe_2O_3, K_2O, etc. with a low Si/Al molar ratio (SAR) of 1.5. To enhance the utilization of coal gangue for SSZ-13 synthesis, an efficient treatment strategy was first developed to activate coal gangue and improve its SAR, which involves a three-step procedure including calcination, ball-milling and acid dealumination (named CBA method, Scheme 1). The calcination process removes the residual carbon from the raw coal gangue and transforms the kaolinite phase into the active metakaolinite phase. Ball milling further reduces the particle size of the calcined coal gangue. Both treatments are beneficial for the subsequent acid leaching processes for aluminum removal.

From Fig. S1 and Table S1, the dealuminated coal gangue (named deAl-G) has particle sizes of about 1 μm, which is amorphous solid except the remaining of residual quartz. The SAR of deAl-G can reach as high as 23.7 under the conditions investigated. Fig. 1 and S1f present the ^{29}Si and ^{27}Al MAS NMR, and ^{29}Si-{^{27}Al} S-RESPDOR NMR spectra of coal gangue and deAl-G, revealing the formation of abundant Si-OH and tetrahedral Al species in deAl-G. The appearance of Si-OH defects in deAl-G is also confirmed by FTIR spectrum (Fig. S1g). Moreover, UV Raman spectrum of deAl-G reveals the existence of ring structures (Fig. S1h). These results suggest that deAl-G, which possesses small particle sizes and abundant defects, would be an active source for zeolite synthesis.

3.2. Synthesis and characterization of SSZ-13 and the Al distribution

3.2.1. Synthesis and characterization of SSZ-13

The synthesis of SSZ-13 by utilization of dealuminated coal gangue was carried out with the assistance of embryonic CHA zeolite. As shown in Table 1, SSZ-13 can be readily synthesized at 175 °C for 12 h after under low TMAdaOH dosage of OSDA/Si = 0.045 ~ 0.072.

The OSDA amounts required by this method are clearly lower than those reported in literatures [19–22] (Table S2). Among the SSZ-13 products, samples GS1 and GS2 were obtained by using deAl-G as the sole Si and Al sources. The high SAR of GS1 was consistent with that of its deAl-G source. Given that the dosage of inorganic cation and its ratio to OSDA in the gel may have a significant impact on properties of SSZ-13 [12,13], the Na amount in the gel was tuned based on the system of sample GS3 (OSDA/Si = 0.072). Within the range of Na/Si = 0.036 ~ 0.130, well-crystallized products (samples GS3-GS6) with similar SAR and high yield (86.4–93.0 %) were obtained, and the product Na/Al ratio showed a rising trend with the incremental Na dosage. Further increasing Na dosage (Na/Si = 0.182 for GS7) would cause a decreased product yield and crystallinity. Moreover, it was found that under low OSDA dosage of 0.045 (GS8 and GS9), a relatively low Na dosage facilities the synthesis of SSZ-13, otherwise the crystallization cannot occur. Likely, the high Na/OSDA ratio under conditions of extremely low OSDA dosage restrained the structural-directing ability of OSDA. It is emphasized that the addition of embryonic zeolite solution is important for a successful synthesis, otherwise no crystallization product can

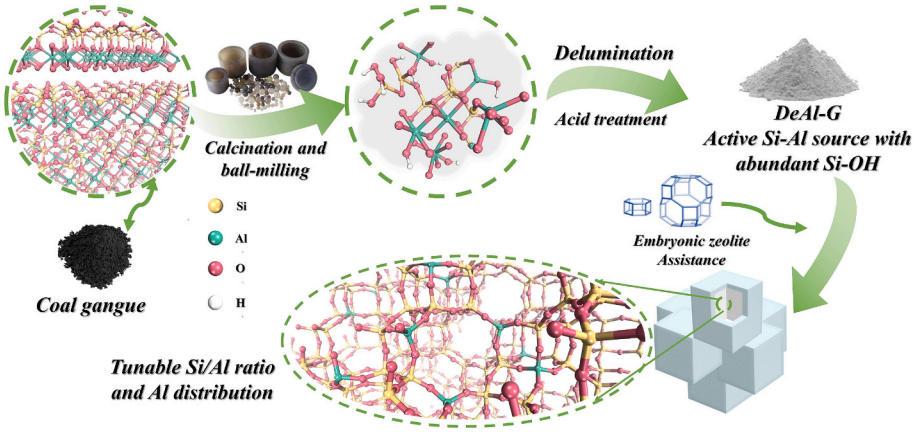

Scheme 1. The schematic of treatment procedure for coal gangue and the synthesis of SSZ-13.

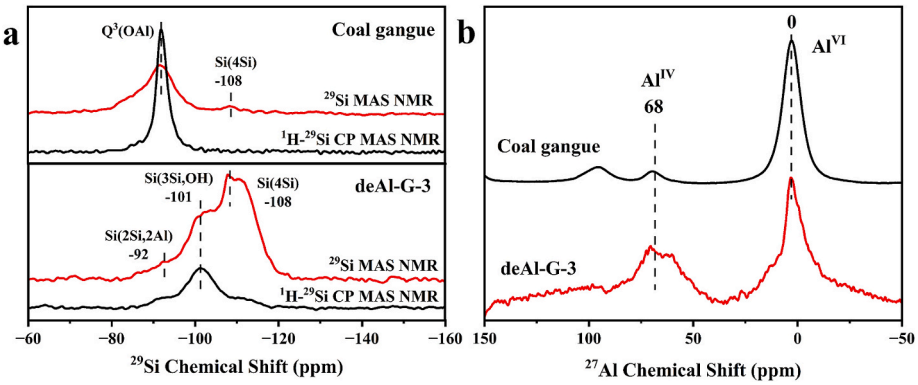

Fig. 1. (a) ^{29}Si MAS NMR (red) and ^{1}H-^{29}Si CP MAS NMR (black) spectra, and (b) ^{27}Al MAS NMR spectra of coal gangue and deAl-G-3 (Si/Al = 9.4).

be obtained (GS10). According to our previous work [18], the abundant double six-membered ring units in embryonic zeolite solution should facilitate the fast nucleation at low alkalinity, and thus contribute to the decrease of OSDA amount required for the synthesis.

The evolution of relative crystallinity and solid yields of samples GS6 and GS8 were investigated and displayed in Fig. 2. The crystallization of GS6 and GS8 can be completed within 5 h and 8 h respectively, with solid yields higher than 90 wt%, showing the remarkable crystallization efficiency of SSZ-13. This implies that deAl-G prepared by CBA method is highly reactive source for zeolite synthesis. Moreover, compared with GS6, the obviously fast crystallization rate of GS8 suggests that relatively low gel alkalinity is beneficial for embryonic solution to exert its effect. These results demonstrate that the present strategy with dealuminated coal gangue as source provides a highly efficient and economic approach for SSZ-13 synthesis.

The XRD patterns of samples GS1-GS8 are shown in Fig. S2a, which can be indexed to the CHA phase with one additional weak peak at near 26° (quartz phase). SEM images of the samples are shown in Fig. S3. With the gradual increase of NaOH dosage in initial gel, the crystal sizes decrease from 2-3 μm to 0.5–1 μm. Additionally, there exist some small particles different from the cubic morphology of SSZ-13. Their SAR was determined to be ~ 193 by TEM-EDS (Fig. S2b), much higher than that of the bulk. In combination of the XRD patterns (Fig. S1c and S2a), these small particles should be inert quartz, resulting from the coal gangue source. The textural properties of the samples are listed in Table S3. Compared with conventional SSZ-13, the micropore area and micropore volume of GS samples are slightly low, likely caused by residue quartz in products. Based on micropore volume, the zeolite content in samples was roughly calculated and given in Table S3. For samples GS3-GS7 with the same receipt except varied NaOH dosage, the zeolite content first rises and then drops following the incremental gel alkalinity. Sample GS6 possesses the highest zeolite content of 97 %.

The acidity of samples H-type GS4-GS7 was measured by NH_3-TPD, and the results are shown in Fig. 3a, Fig. S4 and Table S4. The obviously low acid amount of GS7 is consistent with its low zeolite content as given in Table S3. GS4 and GS5 have approximate acid amounts, which are clearly lower than that of GS6. Specifically, the total acid amount and strong acid amount of GS6 are 1.55 and 1.35 times as much as those of GS4, respectively. The ^{1}H MAS NMR spectra (Fig. 3b, Table S4) also confirm that H-type GS6 possesses more BASs, while H-type GS4 has relatively large amount of Si-OH. As the quartz content of two samples only differs by 6 %, the difference in acid amount may suggest their different dealumination degree during the preparation of H-type samples. Fig. 3c displays the ^{27}Al MAS NMR spectra of the samples. The proportion of non-framework Al in H-type GS4 is clearly higher than that of H-type GS6. Given that the as-made samples possess similar ^{27}Al spectra with tetrahedral Al as main species (Fig. S4), these results evidence the relatively severe dealumination of H-type GS4. In principle, the framework enriched with Al pairs should be more sensitive to the post treatment (e.g. ion exchange). Herein, the better framework stability of H-type GS6 (having more Al pairs than GS4, Table 1) may suggest the higher structural integrity of its parent sample. This speculation is confirmed by FTIR spectra (Fig. S5), showing the larger amount of surface and internal Si-OH on the as-made GS4. It is noted that although H-type GS4 and GS6 have undergone dealumination to some extent, they still maintain high crystallinity (Fig. 3d).

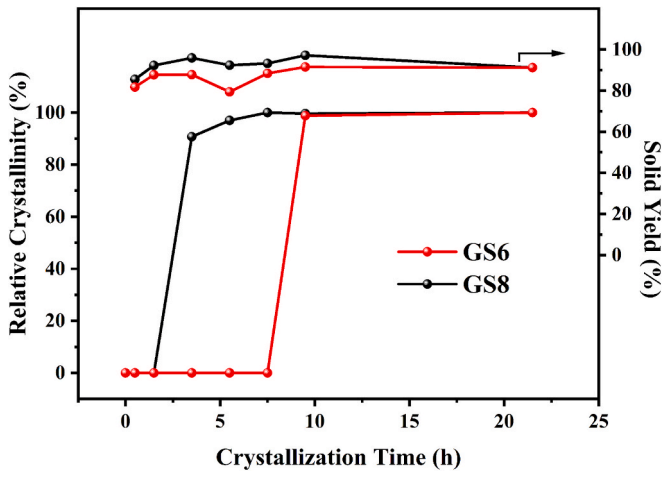

Fig. 2. Evolution of relative crystallinity and solid yields of sample GS6 and GS8.

3.2.2. *Al distribution of SSZ-13*

Co^{2+}-exchange is a widely accepted means to probe the Al distribution. The amount of exchanged Co^{2+} is positively related to the total amount of paired Al (Al_{pairs}) and close unpaired Al (Al_{close}) in zeolites (Fig. S6) [23]. Al_{pairs} represents two Al atoms separated by Si atoms located in one 6-ring or 8-ring, while Al_{close} refers to two Al atoms located in different rings or cavities. The former can accommodate both bare divalent Co(II) cations and Co(II) hexaaqua complexes. However, for Al_{close}, only Co(II) hexaaqua complexes in hydrated zeolites can be accommodated. Detailed definition about them is given in the supporting information (Fig. S6).

Table 1 shows the results of Co exchange capacity of the samples (GS3-GS6). It can be found that the samples synthesized with higher NaOH dosage possess higher Co/Al ratios (the maximum Co/Al = 0.36) and the proportion of isolated Al ($Al_{isolated}$) species shows a decreasing trend. This implies that the Al distribution in the present system can be regulated by adjusting synthesis parameters. Note that the Co/Al ratio of GS6 is at the top level of the reported values (Table S2).

FTIR was further used to detect the T-O-T framework vibration of dehydrated Co^{2+}-exchanged samples to learn the distribution of Al_{pairs}

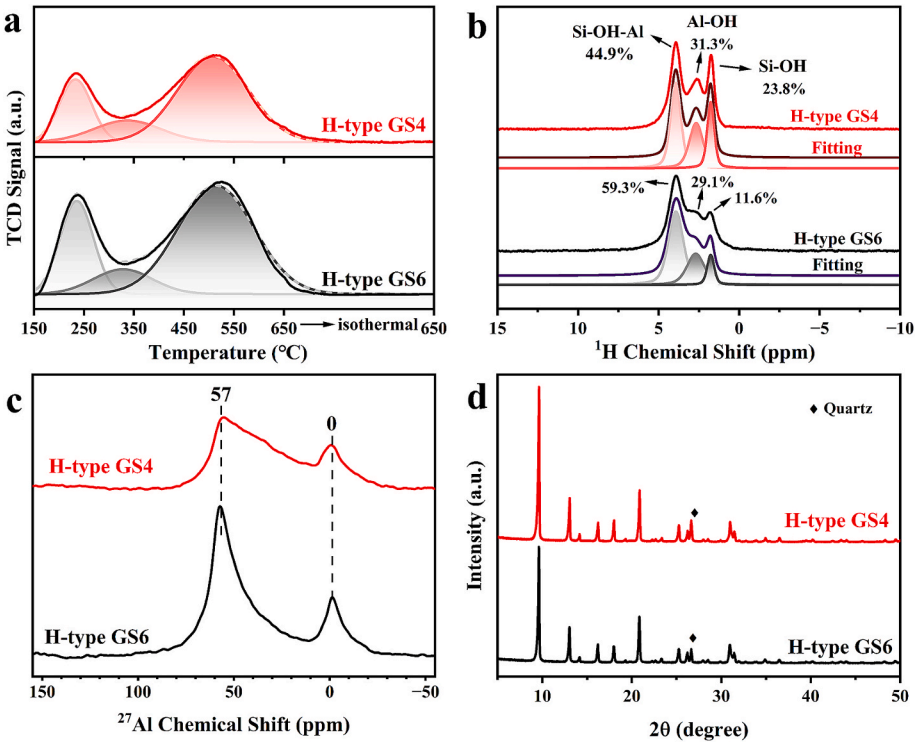

Fig. 3. (a) NH_3-TPD profiles, (b) ^1H MAS NMR spectra, (c) ^{27}Al MAS NMR spectra and (d) XRD patterns of H-type GS4 and GS6.

species (including σ and τ species) [23,24]. As shown in Fig. S6, GS6 possesses a significantly higher proportion of σ-type species (the most stable divalent cation positions located in 6-MR) than GS4. The Al_{pairs} amount (σ + τ) of GS6 is approximately 1.5 times higher than that of GS4. In combination of the Co/Al ratios of the samples (Table 1), the Al_{close} content of GS6 is speculated to be also ~ 1.5 times higher than that of GS4. The results demonstrate that GS6 possesses higher amounts of both Al_{pairs} and Al_{close} than GS4.

3.3. NH_3-SCR performance

A series of gangue-based Cu/SSZ-13 catalysts with different SAR (8.0 ~ 18.5) were first prepared and tested for the NH_3-SCR reaction (Table S5). As shown in Fig. S7, both the low- and high-temperature activities rise following the decrease of the zeolite SAR, implying that the relatively Al-rich sample has better NH_3-SCR catalytic performance. These results are consistent with those reported very recently [7,8,25–27].

Further NH_3-SCR study was thus carried out employing Al-rich catalysts with similar SAR but different Al distribution (Cu/GS4 and Cu/GS6, Cu/Al = 0.22 ~ 0.23). The results are shown in Fig. 4 and S7. Interestingly, under the test conditions of GHSV = 300,000 h^{-1}, Cu/GS6 showed significantly high activity and superior N_2 selectivity. The NO_x conversion can reach 90 % at around 175 ℃, and the T_{90} (NO_x conversion of > 90 %) temperature window was maintained up to 600 °C. Meanwhile, the N_2 selectivity in the entire temperature range is close to 100 %. After hydrothermal aging at 750 ℃ and even 800 ℃ for 16 h, HTA-Cu/GS6 can still maintain wide T_{90} temperature window (250-550℃) and the N_2 selectivity is higher than 90 % at 600 ℃. Fresh Cu/GS4 also presents good NH_3-SCR catalytic performance, but its low- and high-temperature activity was clearly inferior to Cu/GS6. Hydrothermal aged HTA-Cu/GS4 shows a decline in NO_x conversion and N_2 selectivity. The values were inferior to those of HTA-Cu/GS6.

Fig. 5 presents Arrhenius plots of Cu/GS4 and Cu/GS6, and the activation energy (Ea) calculated from the plots. The corresponding NOx conversion profiles of the catalysts are shown in Fig. S8. Cu/GS6 has a comparable apparent Ea with Cu/GS4. The intercept of the plot was defined as pre-exponential factor (A) or frequency factor, which

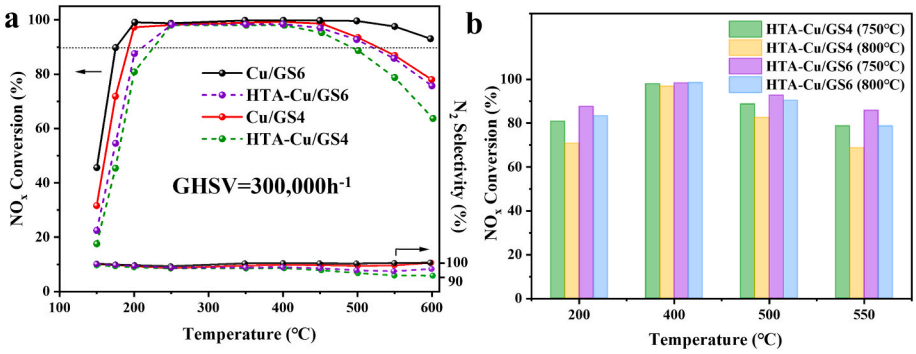

Fig. 4. (a) NH_3-SCR performance of Cu/GS4 and Cu/GS6 before and after hydrothermal aging at 750 °C for 16 h. (b) Comparison of NH_3-SCR activity of aged catalysts. Reaction condition: 500 ppm of NH_3, 500 ppm of NO, 14 % of O_2, 4.5 % of H_2O and N_2 as a balance gas, GHSV = 300,000 h^{-1}. Hydrothermal aging was carried out at 750 or 800 °C for 16 h in 12.5 % H_2O/air with a GHSV of 100,000 h^{-1}.

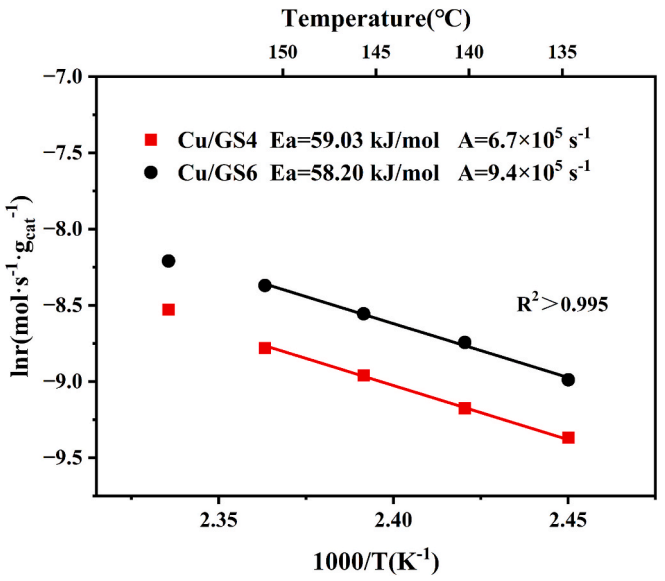

Fig. 5. Arrhenius plots for standard NH_3-SCR in the low-temperature regime of Cu/GS4 and Cu/GS6.

represents the frequency of collisions between reactant molecules and catalytic active sites at a standard concentration. As the Cu contents of the two catalysts are comparable, the relatively high pre-exponential factor for Cu/GS6 means an increased contact probability between reactant molecules and active centers (Cu species and/or acid sites) in the low-temperature catalytic cycles.

3.4. Characterization of Cu/SSZ-13 catalysts

To understand the different low-temperature activities and hydrothermal stability of Cu/GS4 and Cu/GS6, detailed investigation on the textural properties, Cu species and acidity was conducted. Table S6 lists the textural properties of the catalysts, indicating that Cu/GS6 has better structural integrity than Cu/GS4, whatever in fresh and aged forms. The ^{27}Al MAS NMR spectra are shown in Fig. 6. Fresh catalysts present strong resonance at 57 ppm arising from tetrahedral framework Al species. The weak shoulder peak at about 47 ppm implies the existence of twisted four-coordinated Al(IV)-2 species [28], which is considered to be the precursor of extra-framework Al species (EFAL) [29]. Similar NMR signals have been found for zeolites such as MOR, FAU, and MFI [29–32]. After aging, the signal of tetrahedral Al species drops significantly, indicating their great loss. However, the signal around 0 ppm attributed to six-coordinated EFAL did not show an obvious increase. According to previous works [33–35], this phenomenon may be common for Cu/zeolite, owing to the spatial proximity of invisible EFAL with paramagnetic Cu species, or due to increased heterogeneity of Al environments. The corresponding ^{29}Si MAS NMR spectra of the catalysts (Fig. S9) demonstrate that the signal of Si(3Si,1Al) species has an obvious decrease upon aging treatment, which agrees with the serious delamination observed in ^{27}Al NMR spectra. Compared with HTA-Cu/GS4, HTA-Cu/GS6 retains more tetrahedral Al and Si(3Si,1Al) species (Table S7), evidencing the better hydrothermal stability of Cu/GS6.

EPR is a powerful tool for determining the coordination state of isolated Cu^{2+} species through the characteristic g factor and A value of the samples. The g factor is the gyromagnetic ratio of the electron, which can be used to distinguish different electronic states. The A value represents the hyperfine interaction constant, which is used to evaluate the interaction between electron spin and nuclear spin. From Fig. 7, the fresh dehydrated samples have similar Cu^{2+} coordination environments, corresponding to Cu^{2+} coordinated with three or four framework O within 6MR. The small difference in A values may be related to the different Al distributions. Compared with dehydrated samples, hydrated samples have increased g value and reduced A value, which suggest weakened interactions between the framework and hydrated Cu^{2+} ions [36,37]. After hydrothermal aging, the A value of dehydrated samples shows an increase, and there appear new weak peaks near 3450 G and 2950 G, evidencing the evolution of Cu^{2+} coordination environments [33,36]. These weak peaks might associate with the formation of small amount of double Cu^{2+}-2Z species located in one double 6MR [38].

Table 2 lists the quantitative results of different Cu species based on EPR spectra [33,39]. Both fresh catalysts contain Cu^{2+}-2Z and $[Cu(OH)]^+$-Z, but no CuOx species. The higher Cu^{2+}-2Z amount on Cu/GS6 is in agreement with its higher Al_{pairs} content (Fig. S6). However, the Cu^{2+}-2Z/Al ratio on fresh samples is obviously lower than the corresponding Co/Al ratio (Table 1). The reason should be that the formation of $[Cu(OH)]^+$-Z is favorable during the kinetic process of ion exchange, although the Cu^{2+}-2Z species are thermodynamically more stable. $[Cu(OH)]^+$-Z starts to form before the amount of Cu^{2+}-2Z reaches the maximum [26,40]. The distinct Cu distribution of the catalysts is also supported by their different colors (Fig. S10). After hydrothermal aging, Cu^{2+}-2Z species increase together with the formation of CuO_x, while $[Cu(OH)]^+$-Z species disappear, indicating a redistribution of Cu species to more stable sites. The migration and conversion of $[Cu(OH)]^+$-Z to Cu^{2+}-2Z should be owing to the relatively high mobility of $[Cu(OH)]^+$-Z facilitated by water at high temperature. The phenomenon is consistent with previous studies [33,36].

H_2-TPR was performed to investigate the reducibility of Cu^{2+} species (Fig. 8). Fresh catalysts exhibit H_2 consumption in the range of 200–250 °C and 300–350 °C, corresponding to the reduction of Cu^{2+} to Cu^+. They can be attributed to the reduction of $[Cu(OH)]^+$-Z and Cu^{2+}-2Z, respectively [36,41]. Moreover, there are two reduction peaks in the high-temperature range of 450–500 °C and 550–600 °C, attributed to the reduction of Cu^+ to Cu^0. The Cu^+ reduction temperature on Cu/GS6 is about 50 °C higher than on Cu/GS4, indicating a stronger interaction between the framework of GS6 and Cu^+. It is noted that Cu/GS4 displays another weak reduction peak near 750 °C, which is preliminarily

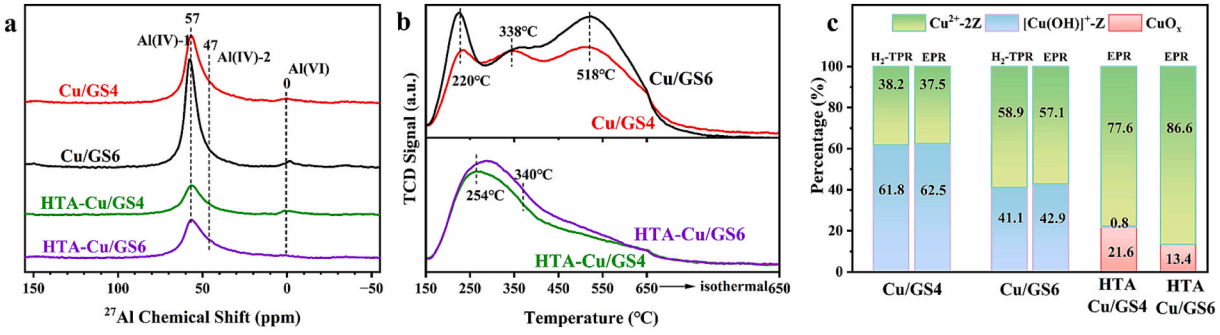

Fig. 6. (a) ^{27}Al MAS NMR spectra and (b) NH_3-TPD curves of the fresh and hydrothermal aging samples. (c) The percentage of different Cu species over the samples determined by EPR and H_2-TPR.

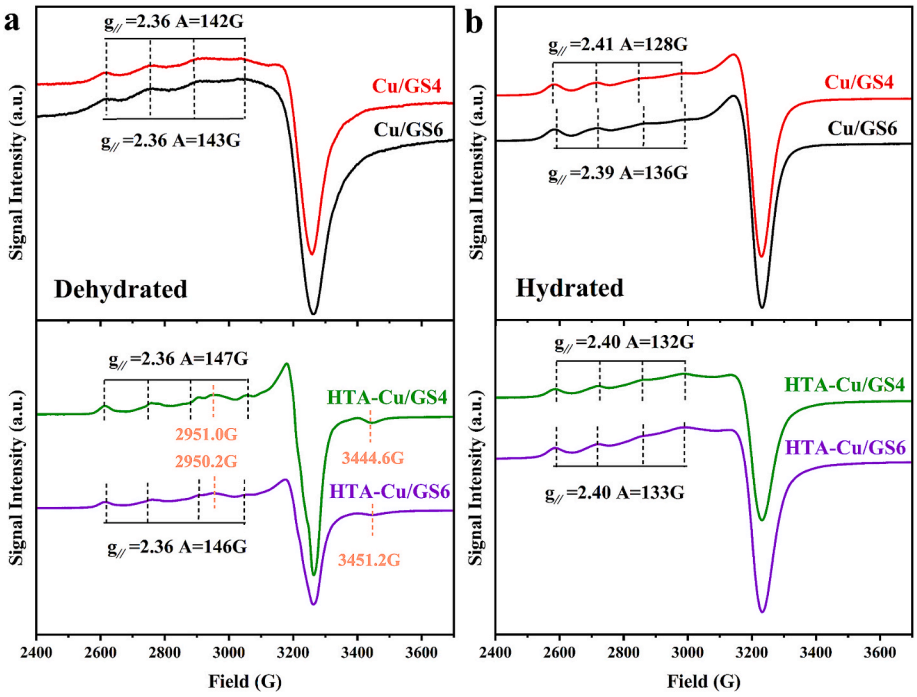

Fig. 7. EPR spectra of the fresh and hydrothermal aging samples. (a) Dehydrated and (b) hydrated samples.

Table 2
Cu distributions on Cu/GS catalysts according to EPR results and the percentage of reducible Cu by H_2-TPR.

Sample	EPR active Cu (wt%)		Cu (wt%)			Cu/Al	Cu^{2+}-2Z/Al	$Cu_{reduced}/Cu_{total}$ [d]
	Hydrated	Dehydrated	Cu^{2+}-2Z [a]	$[Cu(OH)]^+$-Z [b]	CuO_x [c]			
Cu/GS4	2.59	0.97	0.97	1.62	0	0.23	0.09	0.90
Cu/GS6	2.54	1.45	1.45	1.09	0	0.22	0.13	0.91
HTA-Cu/GS4	2.03	2.01	2.01	0.02	0.56	0.23	0.18	0.91
HTA-Cu/GS6	2.20	2.20	2.20	0	0.34	0.22	0.19	0.68

[a] Determined by the EPR spectra of dehydrated samples.
[b] Determined by the difference of EPR results of hydrated and dehydrated samples.
[c] Estimated by the difference of Cu contents determined by XRF and EPR.
[d] Determined by H_2 consumption and Cu content (XRF).

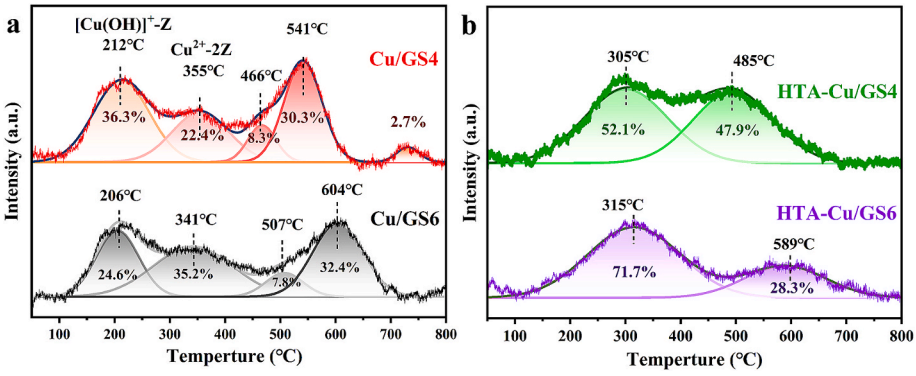

Fig. 8. H_2-TPR profiles of the fresh (a) and hydrothermal aging samples (b).

attributed to the reduction of framework oxygen [42]. Based on the deconvoluted results, fresh Cu/GS6 has a higher proportion of Cu^{2+}-2Z than Cu/GS4, consistent with the EPR results. After aging, both samples show significant changes in H_2-TPR profiles, with two broad peaks appearing around 300 °C and higher temperatures. The former can be attributed to the overlapping reduction of Cu^{2+}-2Z and a small amount of CuO_x species [42], while the latter is related to the reduction of Cu^+ to Cu^0. Furthermore, the reduction temperatures of HTA-Cu/GS6 are higher than those of HTA-Cu/GS4, confirming again the stronger interaction between the framework of GS6 and Cu species.

From Table 2, the reducible Cu species of fresh samples constitutes around 90 % of total Cu. As the reduction area of Cu^{2+} to Cu^+ is larger than that of Cu^+ to Cu^0, it implies that approximately 10 % Cu was not reduced, likely associated with the Cu^+ species interacting strongly with

the framework. After aging, the reducible Cu content on HTA-Cu/GS4 remains unchanged, while the reducibility of Cu^{+} on HTA-Cu/GS6 shows a sharp decrease. The latter may be caused by the redistribution of Cu into special cation sites during reduction treatment [43–45]. Fig. 6c presents the comparison of quantified Cu species based on EPR and H_2-TPR, showing good consistency of the two methods.

The NH_3-TPD results of the catalysts are displayed in Fig. 6b. Cu/GS6 possesses higher amount of weak and strong acid sites than Cu/GS4, similar as those observed for H-type samples. Comparable moderate acid amounts can be perceived for both catalysts. These acid sites are mainly associated with the Cu species [46]. Upon hydrothermal aging, there is a significant loss of strong acid sites, which is in fact a common phenomenon for aged zeolites due to dealumination [41,47,48]. Moreover, the transformation of Cu species from $[Cu(OH)]^{+}$-Z to Cu^{2+}-2Z, as deduced from EPR and H_2-TPR, would also reduce the available BAS due to a consumption of an Al for every Cu moved. The increased mid-temperature peak corresponds to the incremental Cu^{2+}-2Z species (higher NH_3 adsorption capacity). The peak may also include the contribution of Lewis acid sites (LAS) originating from EFAL. Overall, HTA-Cu/GS6 possesses slightly higher amount of acid sites than HTA-Cu/GS4. Fig. S9 presents the FTIR spectra of the catalysts. Fresh Cu/GS6 possesses relatively abundant acidic hydroxyls and lower content of Si-OH. After aging, the acidic hydroxyls of both catalysts show an obvious decline, consistent with the NH_3-TPD results.

According to the above results, although Cu/GS4 and Cu/GS6 possess comparable SAR and Cu/Al ratios, their difference in structural defects and Al distribution, resulted from the variation in synthesis parameters, leads to different Cu species distribution, hydrothermal stability and acidity. Cu/GS6, which has lower defects and higher amount of Al_{pairs} and Al_{close}, Cu^{2+}-2Z and acid amounts, shows better SCR activity and hydrothermal stability.

3.5. Discussion

3.5.1. The importance of Al distribution for low-temperature activity

Cu/GS6 with higher amount of Cu^{2+}-2Z species exhibits better low-temperature NH_3-SCR activity than Cu/GS4 (Table 2, Fig. 4). As $[Cu(OH)]^{+}$ -Z has been demonstrated to have higher mobility and better low-temperature SCR activity than Cu^{2+}-2Z [5,6], the SCR results suggest that the difference in Cu species is not the unique factor determining the low-temperature behavior of the catalysts. It is inferred that Al distribution (acidity) may play important role at low temperatures. To learn the contribution of Al (acid) distribution of the catalysts on NH_3-SCR reaction, Cu/GS catalysts were pre-saturated by NH_3 and then exposed to NO + O_2 at 150 °C. The collected FTIR spectra are shown in Fig. 7. The assignment of the bands associated with NH_3 adsorbed on BAS (B-NH_3) and LAS (L-NH_3) has been labeled in the figure. Following the exposure to NO + O_2 and the consumption of B-NH_3, new bands around 1626, 1597 and 1574 cm^{-1} start to appear, which should be associated with the formation of NO_2, monodentate and bidentate nitrates, respectively [49]. Fig. 9c compares the evolution of the intensity of B-NH_3 species-related signals on the catalysts. Cu/GS6 shows an almost constant decrease rate until the disappearance of the band (t = 60 min). However, Cu/GS4 presents comparable NH_3 consumption rate only in the first 20 min, then the rate significantly slows down. Obvious signals attributed to B-NH_3 can still be observed at t = 60 min. Moreover, the bands associated with nitrates are always more prominent on Cu/GS4 than on Cu/GS6.

According to these results, both the consumption rate of BAS-related NH_3 species and the decomposition of nitrate intermediates on Cu/GS4 are inferior to those on Cu/GS6, implying the importance of the Al (acid) distribution for low-temperature SCR reaction. Given the lower content of $[Cu(OH)]^{+}$-Z and $Al_{isolated}$ species on Cu/GS6 (Table 2 and Fig. S6), the Al species with close spatial proximity (Al_{pairs} and Al_{close}) should be more efficient for the migration of active Cu species. This finding is in consistence with the recent results investigated based on Cu-based zeolitic catalysts with different Al (acid) density [7–9,50].

3.5.2. Understanding the NH_3-SCR performance of aged catalysts

Upon hydrothermal aging, $[Cu(OH)]^{+}$-Z species transferred to thermodynamically stable Cu^{2+}-2Z together with the formation of small amount of CuO_x. Meanwhile, severe dealumination occurred, causing the significant loss of BASs. Both changes led to the decline of low-temperature activity of the catalysts. The low-temperature activity loss on aged catalysts was inferior to the loss of BASs, which suggests that the preservation of active Cu species is more important than that of BASs for SCR reaction. The relatively high conversion on HTA-Cu/GS6 at T ≤ 200 °C should be owing to its larger amount of Cu^{2+}-2Z species.

Decayed NO_x conversion is also observed at T ≥ 450 °C, implying an increased proportion of NH_3 oxidation. Interestingly, HTA-Cu/GS6 shows comparable high-temperature activity as fresh Cu/GS4. Previous works have reported the phenomenon that Cu/SSZ-13 catalysts with more BASs exhibited enhanced NO*x* conversion at high temperature, which suggests an inhibitory effect on NH_3 oxidation [26,51,52]. Herein, given the large amount of BASs on Cu/GS4 and dominant Cu^{2+}-2Z on HTA-Cu/GS6, it is speculated that $[Cu(OH)]^{+}$-Z related species (likely in status of Cu dimers at high temperatures, $2Cu(OH)^{+} \rightarrow Cu\text{-}O\text{-}Cu + H_2O$ [26,53]) have higher activity than Cu^{2+}-2Z for catalyzing NH_3 oxidation. This finding is consistent with the conclusions of Gao and colleagues [40].

3.5.3. Implications for the synthesis control of SSZ-13

The present synthesis results demonstrate that the increase of Na^{+} amount in the initial gel facilitates the generation of Al pairs, which is in line with the findings of previous works [12,13]. The low OSDA dosage in the gel (Table 1) is also believed to enhance the effect of Na^{+} (high Na/OSDA ratio) on inducing the formation of Al pairs, as evidenced by that observed for GS6. On the other hand, relatively high amount of

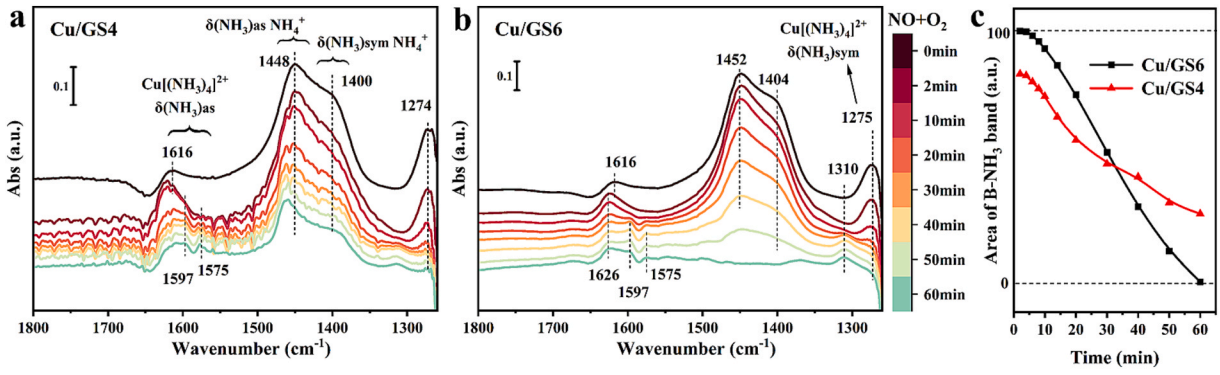

Fig. 9. FTIR spectra of Cu/GS4 (a) and Cu/GS6 (b) exposed to NO + O_2 after being saturated by NH_3 at 150 °C. (c) Intensity comparison of NH_3-BASs species-related signals (1500–1350 cm^{-1}) during the processes.

structural defects was observed in GS4 synthesized with lower alkalinity, which may result from uncomplete condensation of Si/Al species in low alkalinity. The existence of these defects, especially for relatively Al-rich SSZ-13, would result in severe dealumination during the preparation and hydrothermal treatment of Cu-based catalysts, causing the loss of BASs and the decay of SCR activity. It is thus proposed that for the development of highly active and stable zeolite-based SCR catalyst, synthesis efforts should be taken to increase the structural integrity (fewer defects), while constructing relatively high content of Al pairs (to enhance the Cu^{2+}-2Z species).

4. Conclusions

A CBA pretreatment method was developed to prepare dealuminated coal gangue with high reactivity and adjustable composition. By utilizing dealuminated coal gangue as inorganic source, efficient synthesis of SSZ-13 has been achieved with ultra-low TMAdaOH usage and fast crystallization rates (5–12 h). The product Si/Al ratio and framework Al distribution can be facilely tuned by modulating the synthesis parameters. Both fresh and aged Cu/GS6 catalysts exhibit a broad NH_3-SCR working temperature window, demonstrating their superior catalytic performance. It is revealed that the (Al_{pairs} and Al_{close}) species are more effective than $Al_{isolated}$ species for the transfer of active Cu species, which contributes to the excellent low-temperature activity of Cu/GS6. The existence of structural defects aggravate the framework dealumination during catalyst preparation and hydrothermal treatment, and causes decayed catalytic activity. It is proposed that to develop high-performance zeolite catalysts for SCR reaction with enhanced hydrothermal stability, synthesis regulation should be taken to increase the framework Al pairs content and improve the structural integrity (fewer defects).

CRediT authorship contribution statement

Tongrui Liu: Writing – original draft, Validation, Investigation, Formal analysis, Data curation. **Linying Wang:** Writing – review & editing, Visualization, Validation, Funding acquisition, Conceptualization. **Linhai He:** Formal analysis. **Huihui Chen:** Formal analysis. **Dong Fan:** Resources. **Dali Zhu:** Resources. **Miao Yang:** Resources. **Peng Tian:** Writing – review & editing, Visualization, Validation, Supervision, Funding acquisition, Conceptualization. **Zhongmin Liu:** Visualization, Validation, Supervision, Funding acquisition, Conceptualization.

Declaration of competing interest

The authors declare that they have no known competing financial interests or personal relationships that could have appeared to influence the work reported in this paper.

Acknowledgements

This work is supported by National Key Research and Development Program of China (2024YFE0207000) and by the National Natural Science Foundation of China (No. 22288101, 22272171, 22171259, 22272173 and 22302201) and funding from the Sino-French IRN (International Research Network).

Appendix A. Supplementary data

Supplementary data to this article can be found online at https://doi.org/10.1016/j.cej.2025.163003.

Data availability

Data will be made available on request.

References

[1] Z. Bian, J. Dong, S. Lei, H. Leng, S. Mu, H. Wang, The impact of disposal and treatment of coal mining wastes on environment and farmland, Environ. Geol. 58 (2009) 625–634, https://doi.org/10.1007/s00254-008-1537-0.
[2] M. Dusselier, M.E. Davis, Small-pore zeolites: synthesis and catalysis, Chem. Rev. 118 (2018) 5265–5329, https://doi.org/10.1021/acs.chemrev.7b00738.
[3] H. Zhang, P. Han, D. Wu, C. Du, J. Zhao, K.H.L. Zhang, J. Lin, S. Wan, J. Huang, S. Wang, H. Xiong, Y. Wang, Confined Cu-OH single sites in SSZ-13 zeolite for the direct oxidation of methane to methanol, Nat. Commun. 14 (2023) 7705, https://doi.org/10.1038/s41467-023-43508-4.
[4] A.M. Beale, F. Gao, I. Lezcano-Gonzalez, C.H.F. Peden, J. Szanyi, Recent advances in automotive catalysis for NO $_x$ emission control by small-pore microporous materials, Chem. Soc. Rev. 44 (2015) 7371–7405, https://doi.org/10.1039/C5CS00108K.
[5] C. Paolucci, I. Khurana, A.A. Parekh, S. Li, A.J. Shih, H. Li, J.R. Di Iorio, J. D. Albarracin-Caballero, A. Yezerets, J.T. Miller, W.N. Delgass, F.H. Ribeiro, W. F. Schneider, R. Gounder, Dynamic multinuclear sites formed by mobilized copper ions in NO $_x$ selective catalytic reduction, Science 357 (2017) 898–903, https://doi.org/10.1126/science.aan5630.
[6] F. Gao, D. Mei, Y. Wang, J. Szanyi, C.H.F. Peden, Selective catalytic reduction over Cu/SSZ-13: linking homo- and heterogeneous catalysis, J. Am. Chem. Soc. 139 (2017) 4935–4942, https://doi.org/10.1021/jacs.7b01128.
[7] Y. Wu, W. Zhao, S.H. Ahn, Y. Wang, E.D. Walter, Y. Chen, M.A. Derewinski, N. M. Washton, K.G. Rappé, Y. Wang, D. Mei, S.B. Hong, F. Gao, Interplay between copper redox and transfer and support acidity and topology in low temperature NH3-SCR, Nat. Commun. 14 (2023) 2633, https://doi.org/10.1038/s41467-023-38309-8.
[8] S.H. Krishna, A. Goswami, Y. Wang, C.B. Jones, D.P. Dean, J.T. Miller, W. F. Schneider, R. Gounder, Influence of framework Al density in chabazite zeolites on copper ion mobility and reactivity during NOx selective catalytic reduction with NH3, Nat. Catal. 6 (3) (2023) 276–285, https://doi.org/10.1038/s41929-023-00932-5.
[9] Y. Fu, W. Ding, H. Lei, Y. Sun, J. Du, Y. Yu, U. Simon, P. Chen, Y. Shan, G. He, H. He, Spatial Distribution of Brønsted Acid Sites Determines the Mobility of Reactive Cu Ions in the Cu-SSZ-13 Catalyst during the Selective Catalytic Reduction of NOx with NH3, J. Am. Chem. Soc. 146 (2024) 11141–11151, https://doi.org/10.1021/jacs.3c13725.
[10] Y. Cao, D. Fan, D. Zhu, L. Sun, L. Cao, P. Tian, Z. Liu, The effect of Si environments on NH₃ selective catalytic reduction performance and moisture stability of Cu-SAPO-34 catalysts, J. Catal. 391 (2020) 404–413, https://doi.org/10.1016/j.jcat.2020.09.002.
[11] L. Chen, T.V.W. Janssens, P.N.R. Vennestrøm, J. Jansson, M. Skoglundh, H. Grönbeck, A Complete Multisite Reaction Mechanism for Low-Temperature NH $_3$ -SCR over Cu-CHA, ACS Catal. 10 (2020) 5646–5656, https://doi.org/10.1021/acscatal.0c00440.
[12] J.R. Di Iorio, R. Gounder, Controlling the Isolation and Pairing of Aluminum in Chabazite Zeolites Using Mixtures of Organic and Inorganic Structure-Directing Agents, Chem. Mater. 28 (2016) 2236–2247, https://doi.org/10.1021/acs.chemmater.6b00181.
[13] J.R. Di Iorio, S. Li, C.B. Jones, C.T. Nimlos, Y. Wang, E. Kunkes, V. Vattipalli, S. Prasad, A. Moini, W.F. Schneider, R. Gounder, Cooperative and Competitive Occlusion of Organic and Inorganic Structure-Directing Agents within Chabazite Zeolites Influences Their Aluminum Arrangement, J. Am. Chem. Soc. 142 (2020) 4807–4819, https://doi.org/10.1021/jacs.9b13817.
[14] J. Zhang, Y. Shan, L. Zhang, J. Du, H. He, S. Han, C. Lei, S. Wang, W. Fan, Z. Feng, X. Liu, X. Meng, F.-S. Xiao, Importance of controllable Al sites in CHA framework by crystallization pathways for NH3-SCR reaction, Appl. Catal. B Environ. 277 (2020) 119193, https://doi.org/10.1016/j.apcatb.2020.119193.
[15] Y. Wang, J. Han, M. Chen, W. Lv, P. Meng, W. Gao, X. Meng, W. Fan, J. Xu, W. Yan, J. Yu, Low-silica Cu-CHA zeolite enriched with Al pairs transcribed from silicoaluminophosphate seed: synthesis and ammonia selective catalytic reduction performance, Angew. Chem. Int. Ed. 62 (2023) e202306174, https://doi.org/10.1002/anie.202306174.
[16] Q. Ge, M. Moeen, Q. Tian, J. Xu, K. Feng, Highly effective removal of Pb2+ in aqueous solution by Na-X zeolite derived from coal gangue, Environ. Sci. Pollut. Res. 27 (2020) 7398–7408, https://doi.org/10.1007/s11356-019-07412-z.
[17] T. Qian, J. Li, Synthesis of Na-A zeolite from coal gangue with the in-situ crystallization technique, Adv. Powder Technol. 26 (2015) 98–104, https://doi.org/10.1016/j.apt.2014.08.010.
[18] L. Wang, D. Zhu, J. Wang, W. Cui, J. Han, B. Li, D. Fan, P. Tian, Z. Liu, Embryonic zeolite-assisted synthesis of SSZ-13 with superior efficiency and their excellent catalytic performance, J. Mater. Chem. A 9 (2021) 15238–15245, https://doi.org/10.1039/D1TA01452H.
[19] Z. Pourmahdi, H. Maghsoudi, Adsorption isotherms of carbon dioxide and methane on CHA-type zeolite synthesized in fluoride medium, Adsorption 23 (2017) 799–807, https://doi.org/10.1007/s10450-017-9894-1.
[20] B. Wang, L. Ma, L. Han, Y. Feng, J. Hu, W. Xie, W. Bao, L. Chang, Z. Huang, J. Wang, Assembly-reassembly of coal fly ash into Cu-SSZ-13 zeolite for NH3-SCR of NO via interzeolite transformations, Chem. Eng. Sci. X 10 (2021) 100089, https://doi.org/10.1016/j.cesx.2021.100089.
[21] J. Han, X. Jin, C. Song, Y. Bi, Q. Liu, C. Liu, N. Ji, X. Lu, D. Ma, Z. Li, Rapid synthesis and NH $_3$ -SCR activity of SSZ-13 zeolite *via* coal gangue, Green Chem. 22 (2020) 219–229, https://doi.org/10.1039/C9GC02963J.
[22] Q. Zhu, J.N. Kondo, R. Ohnuma, Y. Kubota, M. Yamaguchi, T. Tatsumi, The study of methanol-to-olefin over proton type aluminosilicate CHA zeolites, Microporous

Mesoporous Mater. 112 (2008) 153–161, https://doi.org/10.1016/j.micromeso.2007.09.026.
[23] K. Mlekodaj, J. Dedecek, V. Pashkova, E. Tabor, P. Klein, M. Urbanova, R. Karcz, P. Sazama, S.R. Whittleton, H.M. Thomas, A.V. Fishchuk, S. Sklenak, Al Organization in the SSZ-13 Zeolite. Al Distribution and Extraframework Sites of Divalent Cations, J. Phys. Chem. C 123 (2019) 7968–7987. https://doi.org/10.1021/acs.jpcc.8b07343.
[24] Z. Chen, T. Ye, H. Qu, T. Zhu, Q. Zhong, Progressive regulation of Al sites and Cu distribution to increase hydrothermal stability of hierarchical SSZ-13 for the selective catalytic reduction reaction, Appl. Catal. B Environ. 303 (2022) 120867, https://doi.org/10.1016/j.apcatb.2021.120867.
[25] Y.J. Kim, J.K. Lee, K.M. Min, S.B. Hong, I.-S. Nam, B.K. Cho, Hydrothermal stability of CuSSZ13 for reducing NOx by NH3, J. Catal. 311 (2014) 447–457, https://doi.org/10.1016/j.jcat.2013.12.012.
[26] F. Gao, N. Washton, Y. Wang, M. Kollar, J. Szanyi, C. Peden, Effects of Si/Al ratio on Cu/SSZ-13 NH₃-SCR catalysts: implications for the active Cu species and the roles of Brønsted acidity, J. Catal. 331 (2015) 25–38, https://doi.org/10.1016/j.jcat.2015.08.004.
[27] Y. Shan, J. Du, Y. Zhang, W. Shan, X. Shi, Y. Yu, R. Zhang, X. Meng, F.-S. Xiao, H. He, Selective catalytic reduction of NOxwith NH3: opportunities and challenges of Cu-based small-pore zeolites, Natl. Sci. Rev. 8 (10) (2021) nwab010, https://doi.org/10.1093/nsr/nwab010.
[28] B. Fan, D. Zhu, L. Wang, S. Xu, Y. Wei, Z. Liu, Dynamic evolution of Al species in the hydrothermal dealumination process of CHA zeolites, Inorg. Chem. Front. 9 (2022) 3609–3618, https://doi.org/10.1039/D2QI00750A.
[29] K. Chen, S. Horstmeier, T. Vy, B. Nguyen, S.P. Wang, T. Crossley, Z. Pham, I. Gan, J.L.W. Hung, Structure and catalytic characterization of a second framework Al(IV) site in zeolite catalysts revealed by NMR at 35.2 T, J. Am. Chem. Soc. 142 (2020) 7514–7523, https://doi.org/10.1021/jacs.0c00590.
[30] T.-H. Chen, K. Houthoofd, P.J. Grobet, Toward the aluminum coordination in dealuminated mordenite and amorphous silica–alumina: A high resolution 27Al MAS and MQ MAS NMR study, Microporous Mesoporous Mater. 86 (2005) 31–37, https://doi.org/10.1016/j.micromeso.2005.07.005.
[31] Z. Yu, A. Zheng, Q. Wang, L. Chen, J. Xu, J.-P. Amoureux, F. Deng, Insights into the Dealumination of Zeolite HY Revealed by Sensitivity-Enhanced 27Al DQ-MAS NMR Spectroscopy at High Field, Angew. Chem. 1, Angew. Chem. 122 (46) (2010) 8839–8843, https://doi.org/10.1002/ange.201004007.
[32] K. Chen, Z. Gan, S. Horstmeier, J.L. White, Distribution of Aluminum Species in Zeolite Catalysts: 27Al NMR of Framework, Partially-Coordinated Framework, and Non-Framework Moieties, J. Am. Chem. Soc. 143 (2021) 6669–6680, https://doi.org/10.1021/jacs.1c02361.
[33] J. Song, Y. Wang, E.D. Walter, N.M. Washton, D. Mei, L. Kovarik, M.H. Engelhard, S. Prodinger, Y. Wang, C.H.F. Peden, F. Gao, Toward Rational Design of Cu/SSZ-13 Selective Catalytic Reduction Catalysts: Implications from Atomic-Level Understanding of Hydrothermal Stability, ACS Catal. 7 (2017) 8214–8227, https://doi.org/10.1021/acscatal.7b03020.
[34] S. Prodinger, M.A. Derewinski, Y. Wang, N.M. Washton, E.D. Walter, J. Szanyi, F. Gao, Y. Wang, C.H.F. Peden, Sub-micron Cu/SSZ-13: synthesis and application as selective catalytic reduction (SCR) catalysts, Appl. Catal. B Environ. 201 (2017) 461–469, https://doi.org/10.1016/j.apcatb.2016.08.053.
[35] J.H. Kwak, D. Tran, S.D. Burton, J. Szanyi, J.H. Lee, C.H.F. Peden, Effects of hydrothermal aging on NH₃-SCR reaction over Cu/zeolites, J. Catal. 287 (2012) 203–209, https://doi.org/10.1016/j.jcat.2011.12.025.
[36] Y. Zhang, Y. Peng, J. Li, K. Groden, J.-S. McEwen, E.D. Walter, Y. Chen, Y. Wang, F. Gao, Probing Active-Site Relocation in Cu/SSZ-13 SCR Catalysts during Hydrothermal Aging by In Situ EPR Spectroscopy, Kinetics Studies, and DFT Calculations, ACS Catal. 10 (16) (2020) 9410–9419, https://doi.org/10.1021/acscatal.0c01590.
[37] P.J. Carl, S.C. Larsen, EPR Study of Copper-Exchanged Zeolites: Effects of Correlated *g* - and *A* -Strain, Si/Al Ratio, and Parent Zeolite, J. Phys. Chem. B 104 (2000) 6568–6575, https://doi.org/10.1021/jp000015j.
[38] S.S. Eaton, K.M. More, B.M. Sawant, G.R. Eaton, Use of the ESR half-field transition to determine the interspin distance and the orientation of the interspin vector in systems with two unpaired electrons, J. Am. Chem. Soc. 105 (1983) 6560–6567, https://doi.org/10.1021/ja00360a005.
[39] A. Godiksen, F.N. Stappen, P.N.R. Vennestrøm, F. Giordanino, S.B. Rasmussen, L. F. Lundegaard, S. Mossin, Coordination environment of copper sites in Cu-CHA zeolite investigated by electron paramagnetic resonance, J. Phys. Chem. C 118 (2014) 23126–23138, https://doi.org/10.1021/jp5065616.
[40] F. Gao, E.D. Walter, E.M. Karp, J. Luo, R.G. Tonkyn, J.H. Kwak, J. Szanyi, C.H. F. Peden, Structure–activity relationships in NH3-SCR over Cu-SSZ-13 as probed by reaction kinetics and EPR studies, J. Catal. 300 (2013) 20–29, https://doi.org/10.1016/j.jcat.2012.12.020.
[41] F. Gao, Y. Wang, N.M. Washton, M. Kollár, J. Szanyi, C.H.F. Peden, Effects of alkali and alkaline earth cocations on the activity and hydrothermal stability of Cu/SSZ-13 NH₃–SCR catalysts, ACS Catal. 5 (2015) 6780–6791, https://doi.org/10.1021/acscatal.5b01621.
[42] H. Jiang, B. Guan, X. Peng, R. Zhan, H. Lin, Z. Huang, Influence of synthesis method on catalytic properties and hydrothermal stability of Cu/SSZ-13 for NH3-SCR reaction, Chem. Eng. J. 379 (2020) 122358, https://doi.org/10.1016/j.cej.2019.122358.
[43] Y. Ma, X. Wu, S. Cheng, L. Cao, L. Liu, Y. Xu, J. Liu, R. Ran, Z. Si, D. Weng, Relationships between copper speciation and Brønsted acidity evolution over Cu-SSZ-13 during hydrothermal aging, Appl. Catal. Gen. 602 (2020) 117650, https://doi.org/10.1016/j.apcata.2020.117650.
[44] J.E. Schmidt, R. Oord, W. Guo, J.D. Poplawsky, B.M. Weckhuysen, Nanoscale tomography reveals the deactivation of automotive copper-exchanged zeolite catalysts, Nat. Commun. 8 (2017) 1666, https://doi.org/10.1038/s41467-017-01765-0.
[45] J.D. Albarracin-Caballero, I. Khurana, J.R.D. Iorio, A.J. Shih, J.E. Schmidt, M. Dusselier, M.E. Davis, A. Yezerets, J.T. Miller, F.H. Ribeiro, R. Gounder, Structural and kinetic changes to small-pore Cu-zeolites after hydrothermal aging treatments and selective catalytic reduction of NOx with ammonia, React. Chem. Eng. 2 (2) (2017) 168–179, https://doi.org/10.1039/C6RE00198J.
[46] I. Lezcano-Gonzalez, U. Deka, B. Arstad, A.-V.-Y.-D. Deyne, K. Hemelsoet, M. Waroquier, V.V. Speybroeck, B.M. Weckhuysen, A.M. Beale, Determining the storage, availability and reactivity of NH3 within Cu-Chabazite-based Ammonia Selective Catalytic Reduction systems, Phys. Chem. Chem. Phys. 16 (2013) 1639–1650, https://doi.org/10.1039/C3CP54132K.
[47] J. Luo, F. Gao, K. Kamasamudram, N. Currier, C.H.F. Peden, A. Yezerets, New insights into Cu/SSZ-13 SCR catalyst acidity. Part I: Nature of acidic sites probed by NH3 titration, J. Catal. 348 (2017) 291–299, https://doi.org/10.1016/j.jcat.2017.02.025.
[48] J. Luo, K. Kamasamudram, N. Currier, A. Yezerets, NH3-TPD methodology for quantifying hydrothermal aging of Cu/SSZ-13 SCR catalysts, Chem. Eng. Sci. 190 (2018) 60–67, https://doi.org/10.1016/j.ces.2018.06.015.
[49] B.J. Adelman, T. Beutel, G.-D. Lei, W.M.H. Sachtler, Mechanistic cause of hydrocarbon specificity over Cu/ZSM-5 and Co/ZSM-5 catalysts in the selective catalytic reduction of NOx, J. Catal. 158 (1996) 327–335, https://doi.org/10.1006/jcat.1996.0031.
[50] J.D. Bjerregaard, M. Votsmeier, H. Grönbeck, Influence of aluminium distribution on the diffusion mechanisms and pairing of [Cu(NH3)2]+ complexes in Cu-CHA, Nat. Commun. 16 (1) (2025) 603, https://doi.org/10.1038/s41467-025-55859-1.
[51] T. Yu, T. Hao, D. Fan, J. Wang, M. Shen, W. Li, Recent NH3-SCR mechanism research over Cu/SAPO-34 catalyst, J. Phys. Chem. C 118 (13) (2014) 6565–6575, https://doi.org/10.1021/jp4114199.
[52] T. Yu, J. Wang, M. Shen, W. Li, NH3-SCR over Cu/SAPO-34 catalysts with various acid contents and low Cu loading, Catal. Sci. Technol. 3 (12) (2013) 3234–3241, https://doi.org/10.1039/C3CY00453H.
[53] F. Gao, E. Walter, M. Kollar, Y. Wang, J. Szanyi, C. Peden, Understanding ammonia selective catalytic reduction kinetics over Cu/SSZ-13 from motion of the Cu ions, J. Catal. 319 (2014) 1–14, https://doi.org/10.1016/j.jcat.2014.08.010.